Elastic and Inelastic Cross Sections for Electron-Hg Scattering from Hg Transport Data*

Stephen D. Rockwood
University of California, Los Alamos Scientific Laboratory, Los Alamos, New Mexico 87544
(Received 16 April 1973)

Elastic- and inelastic-scattering cross sections for low-energy electrons in Hg have been obtained through comparison of experimental and calculated transport data. Electron-electron interactions and superelastic collisions are incorporated into the numerical solution for the electron-energy distribution. The electron-electron interactions are shown to have a pronounced effect upon computed drift velocity and characteristic energies at low E/N, while superelastic collisions principally alter the cascade ionization rate. Details of the present method for solving the dc Boltzmann equation, including the above process, are discussed.

I. INTRODUCTION

The search for efficient lasers in the visible and ultraviolet portions of the frequency spectrum has recently generated considerable interest in a class of devices which may be termed dissociation lasers.[1] These laser systems utilize molecules which possess bound excited states and unbound ground states. Molecular Hg_2 is a member of this class of molecules and represents an interesting laser candidate, particularly when one considers the quantity of excited Hg^* produced in electrical discharges. In order to perform a kinetic analysis of the Hg-Hg_2 system it is necessary to have accurate values for the rates of excitation of low-lying states of Hg through electron impact, which in turn requires energy-dependent cross sections for both elastic and inelastic scattering. Contrary to what one might expect, the required cross sections for Hg are not available from the literature; hence, the present investigation has been directed toward generating a self-consistent set of cross sections from transport data following the approach of Phelps and coworkers.[2] The numerical techniques used for solving the dc Boltzmann equation in the present work differ from those of Refs. 2 and 3, and are described in detail in the next sections. It has also been necessary to incorporate electron-electron interactions into the calculation, since most of the characteristic energy data for Hg has been obtained in electrical arcs where account of such collisions is required to make the quoted electron temperature meaningful. Electron-electron interactions were not required in Refs. 2 and 3, and their formulation in the present work will be discussed in the following section.

II. BOLTZMANN EQUATION

A. Basic Formulation

The basic approach for solving the dc Boltzmann equation employed in this investigation extends the formulation of Canavan and Proctor described in Ref. 4. The time evolution of the number density $n(\epsilon, t)\,d\epsilon$ of electrons with energy between ϵ and $\epsilon + d\epsilon$ in a mixture of gases of total number density N is determined by

$$\frac{\partial n}{\partial t} = -\frac{\partial J_f}{\partial \epsilon} - \frac{\partial J_{el}}{\partial \epsilon} + \sum_{s,j} N_s^0 \Big(R_{sj}(\epsilon + \epsilon_{sj}^*)\, n(\epsilon + \epsilon_{sj}^*) + R'_{sj}(\epsilon - \epsilon_{sj}^*) n(\epsilon - \epsilon_{sj}^*) N_s^j / N_s^0 + R_s^i(\epsilon + \epsilon_{si}^*) n(\epsilon + \epsilon_{si}^*) + \delta(\epsilon) \int_{\epsilon_{si}^*}^{\infty} R_s^i(\epsilon)\, n(\epsilon)\, d\epsilon - [R_{sj}(\epsilon) + R'_{sj}(\epsilon) + R_s^i(\epsilon)]\, n(\epsilon) \Big). \quad (1)$$

The first term on the right-hand side of Eq. (1) is the flux of electrons in energy space driven by the applied field E,

$$J_f = \frac{2Ne^2(E/N)^2\epsilon}{3m(\nu/N)} \left(\frac{n}{2\epsilon} - \frac{\partial n}{\partial \epsilon} \right),$$

$$\frac{\nu}{N} = \left(\frac{2\epsilon}{m} \right)^{1/2} \sum_s q_s \sigma_s(\epsilon), \quad (2)$$

where q_s is the mole fraction of species s, $\sigma_s(\epsilon)$ the cross section for momentum transfer from electrons at energy ϵ to molecules N_s, and e and m are the electron charge and mass. The second term on the right-hand side of Eq. (1) is the flux of electrons along the energy axis driven by elastic collisions,

$$J_{el} = \bar{\nu} \left[n \left(\frac{kT}{2} - \epsilon \right) - kT\epsilon \frac{\partial n}{\partial \epsilon} \right], \quad (3)$$

$$\bar{\nu} = 2mN(2\epsilon/m)^{1/2} \sum_s q_s \sigma_s(\epsilon)/M_s,$$

where M_s is the mass of species s and T is the gas temperature. Both fluxes J_f and J_{el} may be noted to contain a current term proportional to $n(\epsilon)$ and a diffusion term proportional to the gradient $dn/d\epsilon$.

The final terms on the right-hand side of Eq. (1) describe the inelastic and superelastic collisions which give rise to nonlocal interactions in energy space. The quantity $R_{sj}(\epsilon)=\sigma_{sj}(\epsilon)v(\epsilon)$ is the rate at which electrons with velocity $v(\epsilon)$ produce excitation from the ground state of species s to excited state j losing energy ϵ^*_{sj} in the processes while $R'_{sj}(\epsilon)=[(\epsilon+\epsilon^*_{sj})/\epsilon]\sigma_{sj}(\epsilon+\epsilon^*_{sj})v(\epsilon)$ is the rate at which electrons at ϵ suffer superelastic collisions with molecules in state N^j_s and gain energy ϵ^*_{sj}. $R^i_s(\epsilon)$ is the ionization rate for species s and the term multiplied by $\delta(\epsilon)$ indicates that all secondary electrons are produced at zero energy. The present formulation of the Boltzmann equation as given by Eq. (1) differs from Eq. (2) of Ref. 2(a) only through the retention of the time dependence and inclusion of the secondary electrons produced by ionization.

Equation (1) is converted to a set of K-coupled ordinary differential equations by finite differencing the electron energy axis into K cells of width $\Delta\epsilon$. From the details as presented in Appendix A one obtains

$$\dot{n}_k = a_{k-1}n_{k-1} + b_{k+1}n_{k+1} - (a_k+b_k)n_k + \sum_{s,j} N_s \Big(R_{sjk+m_{sj}} n_{k+m_{sj}} + R'_{sjk-m_{sj}} n_{k-m_{sj}} N^j_s/N_s + R^i_{sk+m_{si}} n_{k+m_{si}} + \delta_{1k} \sum_m R^i_{sm} n_m - (R_{sjk}+R'_{sjk}+R^i_{sk}) n_k \Big) \tag{4}$$

with

$$a_k = \frac{2Ne^2}{3m}\left(\frac{E}{N}\right)^2 \frac{1}{\nu^+_k/N}\left(\frac{1}{\Delta\epsilon}\right)^2 \left(\epsilon^+_k + \frac{\Delta\epsilon}{4}\right) + \frac{\bar{\nu}_k}{2\Delta\epsilon}\left(\frac{kT}{2} - \epsilon^+_k + \frac{2kT}{\Delta\epsilon}\epsilon^+_k\right),$$

$$b_{k+1} = \frac{2Ne^2}{3m}\left(\frac{E}{N}\right)^2 \frac{1}{\nu^+_k/N}\left(\frac{1}{\Delta\epsilon}\right)^2 \left(\epsilon^+_k - \frac{\Delta\epsilon}{4}\right) + \frac{\bar{\nu}_k}{2\Delta\epsilon}\left(\epsilon^+_k - \frac{kT}{2} + \frac{2kT}{\Delta\epsilon}\epsilon^+_k\right).$$

a_k is interpreted as the rate at which electrons at energy ϵ_k are promoted to energy ϵ_{k+1}, while b_k is the rate for demotion from ϵ_k to ϵ_{k-1}. Notice that all the rates a_k, b_k, R_{sjk}, R'_{sjk} are constants which only need to be evaluated once per calculation.

Equation (4) may be expressed in matrix notation as

$$\dot{n}_k = \sum_l C_{kl} n_l, \tag{5}$$

where the elements of the matrix C_{kl} are readily identified.

When the excited-state populations N^j_s are negligible an important simplification occurs, for now all the elements of $\underline{C}$ are constants and furthermore $\underline{C}$ has upper Hessenberg form with only one diagonal of nonzero elements below the principal diagonal.[5] In this case in the present work, an implicit Euler algorithm is applied to Eq. (5) such that

$$(\underline{I} - \underline{C}\,h)\cdot\vec{n}(t+h) = \vec{n}(t), \tag{6}$$

where $I_{ij}=\delta_{ij}$ is the identity matrix and h is an integration time step. Since the matrix $(\underline{I}-\underline{C}\,h)$ is a constant if h is constant, the problem is converted to solving a set of linear algebraic equations to obtain $\vec{n}(t+h)$ given $\vec{n}(t)$. This is readily accomplished by converting $(\underline{I}-\underline{C}\,h)$ to upper triangular form using column pivoting and solving for $n(t+h)$ by back substitution explicitly accounting for the fact that $(\underline{I}-\underline{C}\,h)$ is an upper Hessenberg matrix.[5] In practice, the convergence properties of this relaxation scheme have proven to be extremely good for arbitrary choices of $\vec{n}(0)$. The calculation of one steady-state distribution on a 300-point energy grid typically requires ~2 sec on a CDC 7600.

If superelastic collisions are not negligible, then $\underline{C}$ is no longer a sparse matrix of upper Hessenberg form. However, if its elements are constants, Eq. (6) still represents a system of linear equations and may be solved by converting $\underline{C}$ to upper triangular form and using back substitution.

To maintain the linearity of Eq. (4) it is necessary to assume that the excited-state populations N^j_s do not vary during the time the electron distribution n_k relaxes to steady state. In practice this is a very good approximation, since the time scale for establishing a steady-state electron distribution is set by the electron neutral collision frequency, which is typically a few picoseconds with neutral densities of $N_s \approx 10^{19}$ cm^{-3}, while the time scale for molecular excitation in glow discharges is on the order of 100 nsec or longer. The effect of superelastic collisions on the elec-

tron distribution may be evaluated by inputting a selected excited-state population distribution N_s^j and observing the resulting equilibrium n_k. In most cases of interest the effect is quite small, as will be discussed in Sec. III. The coupled solution for self-consistent electron and excitation distributions has also been performed as follows: Starting from an initial distribution N_s^j a steady-state electron distribution n_k is computed. From this distribution excitation rates

$$R_s^j = \frac{\int \sigma_{sj}(\epsilon) v(\epsilon) n(\epsilon) d\epsilon}{\int n(\epsilon) d\epsilon} \tag{7}$$

are computed and using these rates the excited-state populations N_s^j are advanced in time by solution of the appropriate rate equations. At a selected time a new steady-state electron distribution is computed using the new values of N_s^j, new rates R_s^j are found and the processes repeated until the system has reached steady state or the desired transient time. This approach of assuming a steady-state electron distribution at each instant in time based upon the instantaneous values of $N_s^j(t)$ has the advantage of filtering out the very rapid relaxation processes in the electron distribution and allows the entire calculation to proceed with a time scale set only by the rate equation governing $\dot{N}_s^j$.

B. Electron-Electron Interactions

For conditions of low E/N and high fractional ionization, electron-electron (e-e) interactions will become important and tend to drive the distribution function towards a Maxwellian. Since the conditions stated above may be expected in arcs and much of the characteristic energy data for Hg is derived from arcs it has been necessary to include e-e interactions in the calculation. Having observed the useful numerical properties of formulating the time rate of change of a quantity as the negative of the divergence of a flux, the same approach will be followed in the incorporation of e-e interactions into Eq. (4). The details as developed in Appendix B follow the formalism presented by Proctor[6] and show that e-e interactions may be incorporated by adding to a_k and b_k of Eq. (4) the terms

$$a_k' = \sum_l A_{kl} n_l, \quad b_k' = \sum_l B_{kl} n_l. \tag{8}$$

The elements of $\underline{A}$ are computed from Eq. (B7) and modified by Eq. (B13); then $\underline{B}$ is set equal to the transpose of $\underline{A}$ as required by Eq. (B9). This results in a finite-difference formulation of e-e interactions which conserves particles and energy exactly. However, the resulting equations are now nonlinear, for the contraction of the constant matrices $\underline{A}$ and $\underline{B}$ with n_k to obtain a_k' and b_k' must be performed each iteration. The differential equations for $\dot{n}_k$ may be solved by a conventional forward-marching numerical integration scheme, such as an Adam's method,[7] or alternatively, the steady-state solution approached by relaxation techniques. In this investigation the latter approach has been employed using a partially implicit algorithm

$$(\underline{I} - \underline{C}h) \cdot \vec{n}(t+h) = [\underline{I} + h\underline{T}(\vec{n})] \cdot \vec{n}(t) \tag{9}$$

where $\underline{T}(n(t))$ is a tridiagonal matrix with elements a' and b' describing e-e interactions. The utility of Eq. (9) lies primarily in the fact the large matrix $(\underline{I} - \underline{C}h)$ is only triangularized once per calculation.

C. Computational Diagnostics

The principal diagnostic employed to assess the validity of the numerical solutions has been energy conservation. Refer to Eq. (4) and note that the first term in the expressions for a_k and b_{k+1} governs the rate at which electrons exchange energy with the dc electric field. Defining the terms $\bar{a}_k$ and $\bar{b}_k$ as

$$\bar{a}_k = \frac{2Ne^2}{3m}\left(\frac{E}{N}\right)^2 \frac{1}{\nu_k^+/N}\left(\frac{1}{\Delta\epsilon}\right)^2 \left(\epsilon_k^+ + \frac{\Delta\epsilon}{4}\right) \tag{10}$$

and

$$\bar{b}_{k+1} = \frac{2Ne^2}{3m}\left(\frac{E}{N}\right)^2 \frac{1}{\nu_k^+/N}\left(\frac{1}{\Delta\epsilon}\right)^2 \left(\epsilon_K^+ - \frac{\Delta\epsilon}{4}\right), \tag{11}$$

the rate of energy gained by the electrons from the dc field is then given by

$$\dot{E}_g = \sum_k (\bar{a}_k - \bar{b}_k) n_k \Delta\epsilon. \tag{12}$$

This energy source is balanced by losses through elastic collisions

$$\dot{E}_{el} = -\sum_k [(a_k - \bar{a}_k) - (b_k - \bar{b}_k)] n_k \Delta\epsilon \tag{13}$$

and inelastic losses

$$\dot{E}_{incl} = \sum_{ksj} (R_{sjk+m_{sj}} n_{k+m_{sj}} N_s m_{sj} + R^i_{sk+m_{si}} n_{k+m_{si}} N_s m_{si} - N_s^j R'_{sjk-m_{sj}} n_{k-m_{sj}} m_{sj}) \Delta\epsilon. \tag{14}$$

For all computations accepted in this investigation the difference between $\dot{E}_g$ and $\dot{E}_{el} + \dot{E}_{incl}$ was less than one part in 10^6.

The coding of the electron-electron interaction was subjected to two test cases. First it was verified that with only e-e interactions, a Maxwellian was indeed a steady-state solution of the

difference equations. Secondly an initially non-Maxwellian distribution containing a known energy density Q, and electron number density n_0, was observed to relax to a Maxwellian distribution with a temperature $kT_e = \frac{2}{3}Q/n_0$.

The transport coefficients which were computed for comparison with experimental data included the drift velocity v_d(cm/sec), the characteristic energy ϵ_k(eV), and the ionization coefficient per molecule α_i/N(cm^2). These parameters are defined as follows:

$$v_d = \dot{E}_\epsilon/(En_0), \quad n_0 = \sum_k n_k, \tag{15}$$

$$\epsilon_k = eD/\mu \tag{16}$$

after Ref. 2 where the mobility

$$\mu = v_d/(E/N) \tag{17}$$

and the diffusion coefficient

$$D = \tfrac{1}{3}(2/m)^{1/2} \sum_k \frac{\epsilon_k f_k \Delta\epsilon}{\sum_s q_s \sigma_s(\epsilon_k)} \tag{18}$$

with

$$f_k = n_k/(\epsilon_k^{1/2}\Delta\epsilon n_0). \tag{19}$$

Finally

$$\frac{\alpha_i}{N} = \frac{\sum_{sk} R_{sk}^i N_s n_k/n_0}{v_d N}, \tag{20}$$

where R_{sk}^i is the ionization rate (cm^3/sec) for species s at energy k.

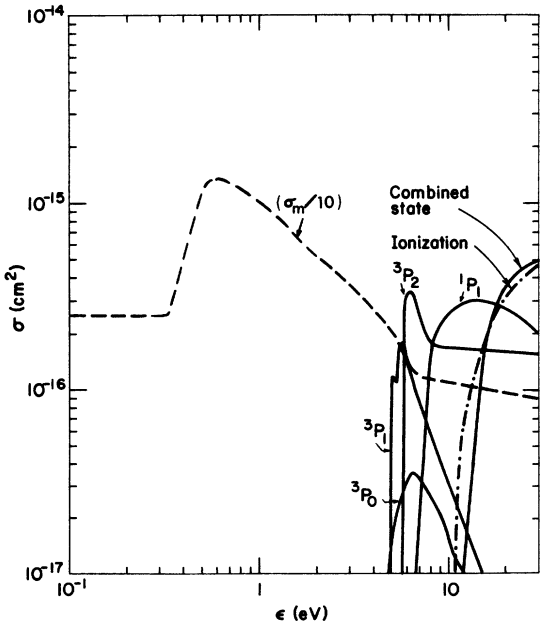

FIG. 1. Elastic- and inelastic-scattering cross sections for electrons in Hg as a function of energy.

III. RESULTS AND DISCUSSION

Exercising the techniques developed in Sec. II, steady-state distributions have been computed in the range $10^{-18} \leq E/N \leq 10^{-14}$ V cm^2. The inelastic processes considered were excitation from the Hg ground state to the $6\,^3P_{0,1,2}$ states, the $6\,^1P_1$ state, a lumped-state representative of higher electronic levels, and ionization. Initial estimates for the required cross sections were obtained from the work of McCutchen[8] for momentum transfer, the data of Borst[9] for near threshold ionization fitted to the results of Harrison[10] for higher energies, and the work of Borst[9] for the $6\,^3P_2$ excitation cross section. The relative cross section obtained by Ottley *et al.*[11] was taken for the $6\,^3P_1$ state and normalized to the $6\,^3P_2$ cross section using the results quoted by von Engel.[12] Initial estimates for the remaining cross sections were also taken from von Engel. Adjusting the initial cross sections for momentum transfer and electronic excitation to the values displayed in Fig. 1 yielded the comparison between computed and experimental v_d and ϵ_k given in Fig. 2. Figure 3 compares the computed ionization coefficient (solid curve) with experimental data. These displayed results represent a best fit with the currently available experimental data. However, as one can observe from Figs. 2 and 3 considerable

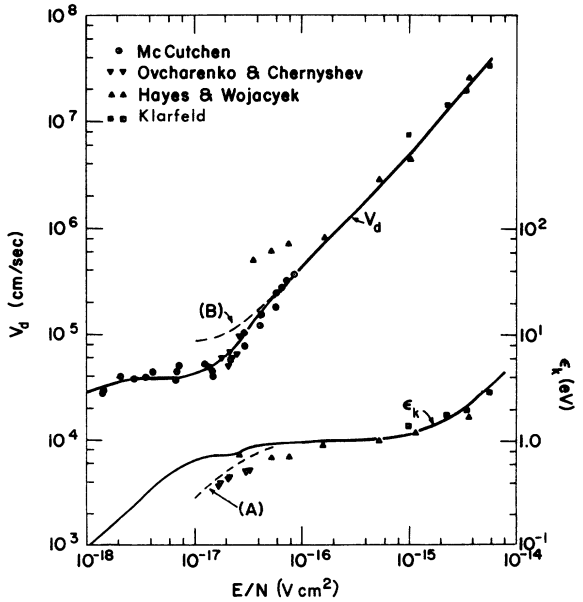

FIG. 2. Comparison of computed values (solid curve) and experimental data from Refs. 8 and 13–15 for drift velocity v_d (cm/sec) and characteristic energy ϵ_k (eV) as a function of E/N (V cm^2).

scatter is present in the data and in particular little data for ϵ_k exist. Since so little data relevant to inelastic scattering were available, the decision was made to assume the ionization cross sections obtained from Borst and Harrison were accurately known and would not be varied. Having made this choice, the values of α_i may be used to determine the magnitude of the excitation cross sections for their values determine the fractional number of electrons which are able to reach the ionization threshold. The method employed herein for obtaining cross sections from transport data can only yield a value for the total excitation cross section at any energy. The partitioning of the total cross section among individual levels requires additional information. In the present case the relative magnitudes of the cross sections given in von Engel have been employed.

The maximum values of the $6\,^3P_{1,2}$ cross sections as given in Fig. 1 are virtually the same as those reported by Kenty in his investigation of Hg-Ar discharges,[19] while the maximum value of the $6\,^3P_0$ cross section used in the present work is smaller by approximately 55%. Notice, however, that the $^3P_0$ cross section is small in comparison to the others, and as a consequence, the total inelastic cross section for $6\,^3P$ excitation in the present work agrees with that of Ref. 19 to within 25% above $\epsilon = 5$ eV.

With the cross sections displayed in Fig. 1 the binary rate for excitation of each level has been computed according to

$$R_j = \sum_k \sigma_j(\epsilon_k) v(\epsilon_k) n_k/n_0 \tag{21}$$

and the results are displayed in Fig. 4. Notice that over the E/N range considered here the $6\,^3P_1$ state receives most of the energy while the excitation of states higher than $6\,^1P_1$ represented by the lumped state accounts for less than 5% of the total excitation energy. As a consequence, the computed transport coefficients are quite insensitive to the behavior of this lumped cross section and the neglect of explicitly following excitation to levels other than the $6P$ states is justified.

The partition of the total energy deposition rate among the various modes of excitation is shown in Fig. 5. Notice that for $E/N \geq 10^{-16}$ V cm^2 virtually all of the energy is going into electronic excitation. Furthermore, Hg is somewhat unique in that the ionization rate remains quite low until very large values of E/N are reached. This gives a wide operating range on E/N for which the dis-

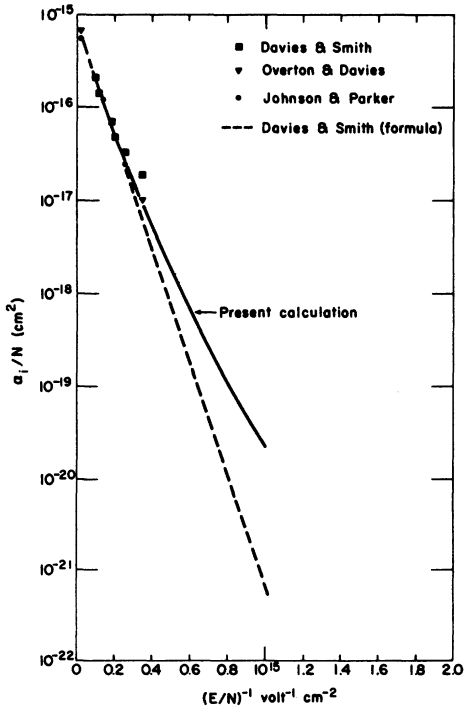

FIG. 3. Comparison of computed values (solid curve) and experimental data from Refs. 16–18 for ionization coefficient per Hg atom, α_i/N (cm^2), as a function of $(E/N)^{-1}$ V^{-1} cm^{-2}.

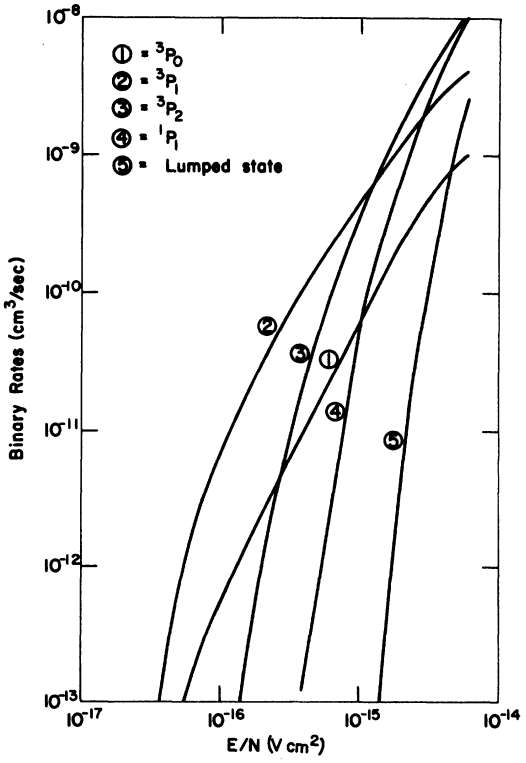

FIG. 4. Computed binary excitation rates R_j (cm^3/sec) to selected excited states of Hg.

charge should remain stable and a maximum amount of energy is given to excited states. These facts make Hg quite attractive as a potentially efficient dissociation laser medium.

To elucidate the manner in which the measured transport coefficients reflect the behavior of the cross sections, consider the details of v_d and ϵ_k displayed in Fig. 2. Beginning from the lowest E/N, v_d and ϵ_k are determined entirely by the functional form of the momentum-transfer cross section σ_m. The plateau in v_d for E/N between 2×10^{-18} and 6×10^{-18} V cm^2 is a result of the rapid rise in σ_m between 0.32 and 0.6 eV. The magnitude of v_d in the plateau and position of the knee in v_d at $E/N\approx10^{-17}$ V cm^2 is quite sensitive to the energy and initial slope of the rise in σ_m. For example, if σ_m is allowed to rise abruptly at 0.2 eV instead of 0.32 eV, then the knee in v_d is shifted to $E/N \approx 6\times10^{-18}$ V cm^2 and the value of v_d drops to 3×10^4 cm/sec in the plateau region. As a consequence of this sensitivity, the values for σ_m between 0 and 1 eV are the most accurately determined cross sections with accuracy limited principally by scatter or absence of experimental data.

As E/N is increased beyond 10^{-17} V cm^2, ϵ_k initially remains bound to a value of 0.7 eV by elastic losses in the large barrier of σ_m. This continues until $E/N\approx3\times10^{-17}$, at which point electrons begin to penetrate the "elastic loss barrier" and the tail of the distribution moves rapidly to values near 4.8 eV where the barrier presented by inelastic losses is encountered. The value of E/N at which ϵ_k begins to rise from its initial plateau is set by the magnitude of the peak in σ_m, while the range in E/N for which ϵ_k is held fixed near the value of $\epsilon_k\approx1$ eV is determined by the absolute magnitude of the inelastic cross sections σ_x.

By comparing a_k [Eq. (4)] to $a_k-\bar{a}_k$ [Eq. (10)], one can derive a simple criteron for the value of E/N at which energy losses to inelastics become important. The resulting requirement is

$$\frac{(2e^2/3m)(E/N)^2(\nu/N)^{-2}}{(4m/M)\epsilon_k}\gtrsim 1. \tag{22}$$

Inserting numerical values appropriate for Hg at $\epsilon_k\approx1$ eV yields $(E/N)^2\gtrsim4\times10^{-34}$ (V cm^2)^2 so that inelastic collisions rapidly become important as E/N increases beyond 2×10^{-17} V cm^2 as observed in Fig. 5.

Continuing with the determination of σ_x, using α_i as another data set as described previously allows one to give a reasonably accurate normalization for the total σ, but individual inelastic-scattering cross sections are not determined when they overlap to the extent present in Hg. If the individual σ_x's were widely spaced in energy, then they could be determined with much higher accuracy.

Throughout the range $E/N\geq3\times10^{-17}$ calculations show v_d to vary as $v_d\sim1/\sigma_m$ so that the magnitude of σ_m at energies greater than ~2 eV is determined by the behavior of v_d.

The total scattering cross section and momentum-transfer cross section at energies $\epsilon>1$ eV obtained from the present calculation are compared with the results of beam transmission ex-

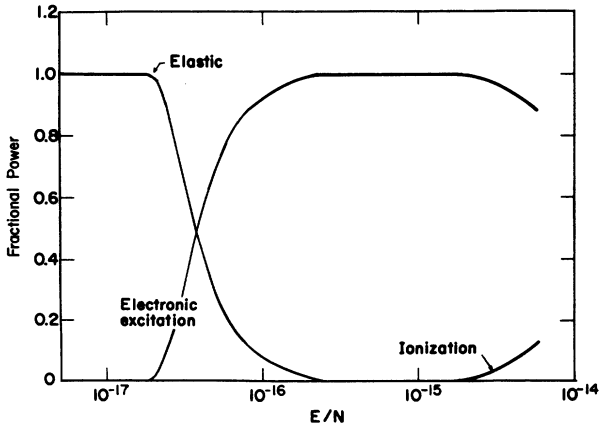

FIG. 5. Fractional partition of total discharge power v_d (E/N) among elastic and inelastic losses as a function of E/N (V cm^2).

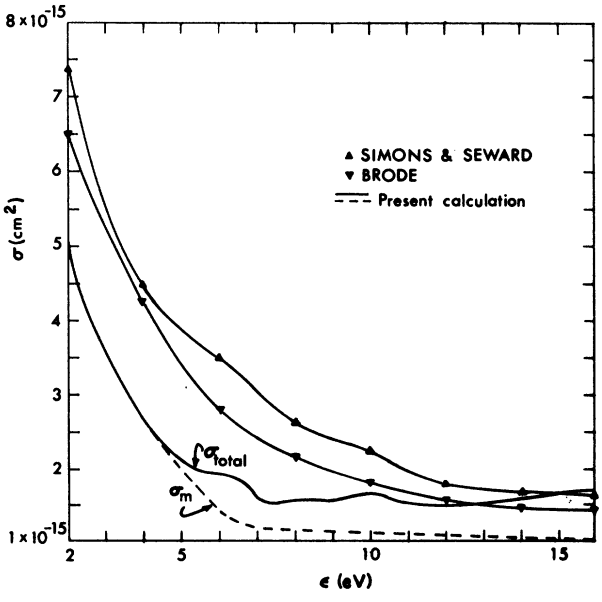

FIG. 6. Comparison of present cross sections with results of low-energy electron-beam transmission experiments.

periments[20,21] in Fig. 6. The present values of σ_m are systematically low over the entire range $2 \leq \epsilon \leq 5$ eV. This may be attributed to the fact that the momentum-transfer cross sections derived in this investigation are sensitive to large-angle scattering, while the geometry of the beam transmission experiments only allows measurements of small-angle scattering. With the onset of the inelastic processes above 5 eV, the present total cross section moves closer to the experimental results. The coincidence of inflections in the measured cross section of Ref. 21 and the present work at $\epsilon \approx 6.5$ and 10 eV is intriguing; however, one must be cautioned against assigning a physical significance to this since the present method does not possess the sensitivity at these high energies to predict 10% variations in σ_T.

It remains now to assess the extent to which e-e interactions alter the computed distributions. Before examining the results of the numerical calculations it is instructive to derive criteria analogous to Eq. (22) which determine when e-e interactions dominate the distribution. Comparing the electron flux in energy space as driven by the field J_f [Eq. (2)] to the flux driven by e-e collisions J_{ee} [Eq. (B6)], one finds that $J_{ee} \gtrsim J_f$ at low ϵ if

$$\frac{e^2}{3m} \frac{(E/N)^2}{p} \frac{1}{\nu/N} \frac{\sqrt{\epsilon}}{\alpha} < 1, \tag{23}$$

where $p = n_0/N$ is the fractional ionization and $\alpha \approx 8 \times 10^{-6}$ eV$^{3/2}$ cm^3/sec [Eq. (B1)]. Numerically Eq. (23) gives 10^{27} (V cm^2)$^{-2} \times (E/N)^2 < p$ with $\epsilon \sim 1$ eV, which indicates that at $E/N = 10^{-16}$ V cm^2 e-e interactions become a dominant factor if $p > 10^{-5}$. Notice that the value of p required to satisfy Eq. (23) approached 0 as $\sqrt{\epsilon} \sim 0$. At higher energies, one should compare $\partial J_{ee}/\partial \epsilon$ to contributions in $\dot{n}(\epsilon)$ produced by inelastic collisions. This results in a third criteron:

$$p > (v \epsilon^{1/2} \epsilon_k/\alpha)\, \sigma_x(\epsilon) \approx 10^{13} (\text{cm}^{-2}) \times \sigma_x(\epsilon) \tag{24}$$

which states that if $\sigma_x \approx 10^{-16}$ cm^2 then fractional ionizations $p \gtrsim 10^{-3}$ will be sufficient to thermalize the entire distribution.

The semiquantitative arguments presented above are borne out by the results of detailed numerical calculations including e-e collisions as described in Appendix B. Figure 7 displays a series of computed electron distributions f_k [Eq. (19)] for

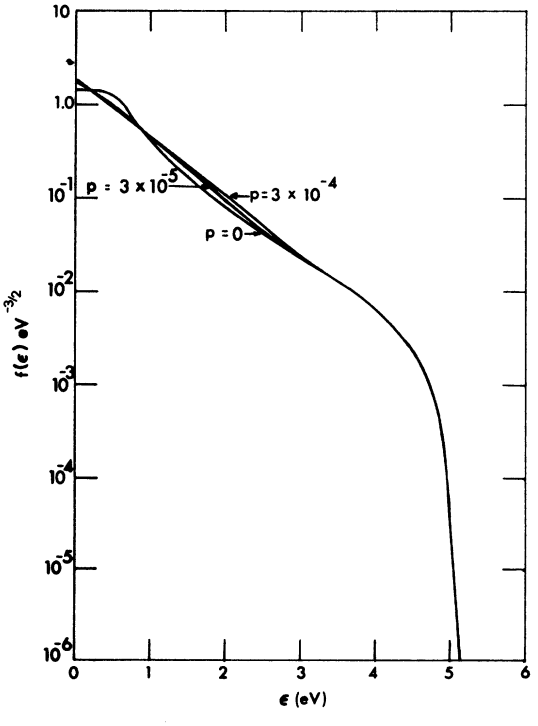

FIG. 7. Computed electron distributions $f(\epsilon)$ (eV$^{-3/2}$) including electron-electron interactions for selected fractional ionization p. Electron-ion collisions should be included for $p > 4 \times 10^{-4}$.

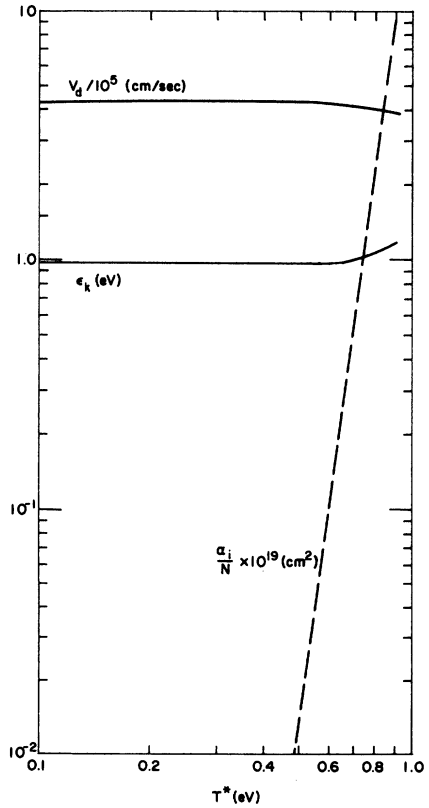

FIG. 8. Computed drift velocity v_d (cm/sec), characteristic energy ϵ_k (eV), and ionization coefficient α_i/N (cm^2) as a function of excitation temperature T^* (eV).

various fractional ionizations at $E/N = 3\times10^{-17}$ V cm^2. The normalization is $\int f(\epsilon)\epsilon^{1/2}d\epsilon = 1$, and on this plot a Maxwellian distribution would appear as a straight line. Notice that as p is increased the e-e collisions alter the low-energy portion of the distribution first. This is to be expected because of the $\epsilon^{-1/2}$ dependence of the e-e interaction. By a value of $p = 10^{-4}$, which is typical of the experimental conditions of Ref. 13, the electron distribution has thermalized toward a Maxwellian out to energies $\epsilon = 4.0$ eV. However, beyond 4.8 eV where inelastic losses are important, the distribution functions remain unaltered. These results are in keeping with simple expectations of Eq. (23) and (24). The value of ϵ_k from the curve $p = 3\times10^{-4}$ of Fig. 7 has decreased from its value obtained when the e-e interactions were neglected. In fact, for a value of p typical of Ref. 13, one obtains values of ϵ_k vs E/N given by curve A of Fig. 2 which are in good agreement with the experimental results. The thermalization of the distribution due to e-e interactions is sufficient to overcome the elastic loss barrier, and in contrast to the solid curve of Fig. 2, no plateau in ϵ_k is observed when $p = 3\times10^{-4}$ (curve A). While the computed and experimental values of ϵ_k compare favorably, the values of v_d (curve B, Fig. 2) do not. The computed drift velocities at $E/N \approx 2\times10^{-17}$ and $p = 3\times10^{-4}$ lie above the experimental data of Ref. 13. It has not been possible to obtain a set of cross sections which yield v_d and ϵ_k consistent with both the experimental results of Ref. 8 (where e-e interactions are unimportant) and Ref. 13 (where e-e interactions must be included). The effect of e-e interactions in low-pressure Hg discharges has recently been examined by Atajew *et al.*[22] The two calculations are not in good agreement at low E/N. In particular, in Ref. 22, values of v_d for $E/N < 10^{-17}$ fall below the present values, shown in Fig. 2, when e-e interactions are neglected. This behavior is qualitatively inconsistent with the occurence of the "jump" in σ_m used in Ref. 22 at a higher energy than shown in Fig. 1. Further disagreement occurs when e-e interactions are included, with Ref. 22 predicting a much greater increase in the mobility at $E/N \approx 10^{-17}$ with increasing p than is found in the present results. The source of these discrepancies is not known, but could arise from zoning along the energy axis. The present calculation has typically used a $\Delta\epsilon = 0.01$ eV and found the computed transport data to be independent of $\Delta\epsilon$ for $\Delta\epsilon < 0.02$ eV with $10^{-18} < E/N < 10^{-17}$.

The final process to be considered is the effect superelastic collisions have upon the computed transport data. To perform this analysis in detail would require the development of an accurate kinetic model for Hg. This has not been the object of this study, so, as an alternative, the excited-state populations of Hg have been assumed to obey a Maxwellian distribution with a temperature T^*. Then for a given E/N, the behavior of v_d and ϵ_k as a function of T^* has been investigated. The results for $E/N = 10^{-16}$ V cm^2 are displayed in Fig. 8. Notice that v_d and ϵ_k are virtually independent of T^* until T^* is within 60% of the nominal value of ϵ_k from Fig. 2. At this point, ϵ_k begins to rise, owing to the cancellation of excitation losses by superelastic collisions. At the same time, v_d decreases, reflecting a decrease in the mobility as a consequence of the increased collision frequency. It should be noted that ϵ_k and v_d reflect the behavior of the bulk of the electron distribution and, while they are insensitive to T^*, this is not true of α_i. The ionization rate depends critically upon the high-energy tail of the distribution which, in turn, is quite sensitive to T^*. For example, when $T^* = 0.3$ eV, α_i has already increased by a factor of 10^3 over its value at $T^* = 0.1$ eV and continues to rise rapidly thereafter, as shown in Fig. 8. Ionization from excited states has not been included in the calculation. However, as mentioned in Ref. 19, this will produce an additional increase in α_i for large values of T^*. This combined behavior could have a significant effect upon the stability of a discharge operating near the breakdown limit.

In summary, elastic and inelastic scattering cross sections for low-energy electrons in Hg have been obtained which are consistent with available transport data. The numerical calculations have included electron-electron interactions and superelastic collisions with the former proving to significantly alter the bulk of the computed distribution function at low E/N, while the latter principally effects α_i. From the method used here, the elastic scattering cross section for $0 < \epsilon < 4$ eV is determined to within the scatter of experimental data. Likewise, the magnitude of the total inelastic cross section is well determined near threshold; however, the partition between various excitation processes is much less certain. Inelastic cross sections above $\epsilon = 25$ eV are not determined by this method, for discharges in the E/N range considered here contain a negligible number of electrons beyond $\epsilon = 25$ eV.

ACKNOWLEDGMENT

The author wishes to gratefully acknowledge the support of Dr. A. V. Phelps who graciously supplied information on Hg transport data.

APPENDIX A

When the time-dependent Boltzmann equation represented by Eq. (1) is projected onto a finite-differenced energy axis containing K cells of width $\Delta\epsilon$, there results a set of K coupled first-order differential equations

$$\dot{n}_k = -\frac{[J_f^+(k) - J_f^-(k)]}{\Delta\epsilon} - \frac{[J_{el}^+(k) - J_{el}^-(k)]}{\Delta\epsilon} + \sum_{s,j} N_s \Big(R_{sjk+m_{sj}} + R'_{sjk-m_{sj}} n_{k-m_{sj}} N_s^j/N_s + R^i_{sk+m_{si}} n_{k+m_{si}} + \delta_{1k} \sum_m R^i_{sm} n_m - (R_{sjk} + R'_{sjk} + R^i_{sk}) n_k \Big) \tag{A1}$$

with

$$J_f^+(k) = \frac{2Ne^2}{3m}\left(\frac{E}{N}\right)^2 \frac{\epsilon_k^+}{\nu_k^+/N}\left(\frac{n_{k+1}+n_k}{4\epsilon_k^+} - \frac{n_{k+1}-n_k}{\Delta\epsilon}\right), \tag{A2}$$

$$J_{el}^+(k) = \bar{\nu}_k^+\left[\frac{n_{k+1}+n_k}{2}\left(\frac{kT}{2} - \epsilon_k^+\right) - kT\epsilon_k^+\left(\frac{n_{k+1}-n_k}{\Delta\epsilon}\right)\right], \tag{A3}$$

and

$$\frac{\nu_k^+}{N} = \left(\frac{2\epsilon_k^+}{m}\right)^{1/2} \sum_s q_s \sigma_s(\epsilon_k^+),$$

$$\bar{\nu}_k^+ = 2mN\left(\frac{2\epsilon_k^+}{m}\right)^{1/2} \sum_s \frac{q_s \sigma_s(\epsilon_k^+)}{M_s},$$

where

$$\epsilon_k^+ = k\Delta\epsilon, \quad \epsilon_k^- = \epsilon_{k-1}^+,$$

$$J^-(k) = J^+(k-1), \quad m_{sj} = \epsilon_{sj}^*/\Delta\epsilon.$$

The first two terms on the right-hand side of Eq. (A1) possess the desirable property of conserving the total number of electrons $n_0 = \sum_k n_k$ exactly even in finite-difference form if the physical boundary conditions $J_1^- = J_K^+ = 0$ are employed. The entire equation is then required to conserve particles exactly by setting to zero rates for which $k + m_{sj} > K$ and $k - m_{sj} < 1$. Now substitute Eqs. (A2) and (A3) into Eq. (A1) and perform the indicated algebra, grouping coefficients of n_k, $n_{k\pm1}$ to obtain Eq. (4) of the text.

In the region where only elastic collisions are important, an approximate analytic solution for n_k has been obtained in the form of a Druyvesteyn distribution.[23] It is interesting to note that in this region, one may obtain an analytic solution to the difference equation [Eq. (4)] for $\dot{n}_k = 0$ independent of the form of σ_m. From Eq. (4) with the indicated boundary condition $b_1 = 0$, it is found that

$$n_2 = (a_1/b_2)\, n_1, \tag{A4}$$

which is a function only of $\sigma(\epsilon_1)$. Similarly, setting $\dot{n}_k = 0$, $k \neq 1$ leads to the recursion relation

$$n_{k+1} = \frac{a_k + b_k}{b_{k+1}} n_k - \frac{a_{k-1}}{b_{k+1}} n_{k-1}, \tag{A5}$$

which can be evaluated using Eq. (4), Eq. (A4), and the assumed behavior of $\sigma_m(\epsilon_k)$. The relative values of n_k may then be made absolute using

$$\sum_k n_k = n_0.$$

APPENDIX B

From the work of Rosenbluth *et al.*, one may write, for the case of interactions between free electrons with an isotropic velocity distribution,[24]

$$\frac{\partial n}{\partial t} = \alpha\left[3\epsilon^{-1/2}n^2 + 2\epsilon^{3/2}\frac{\partial\psi}{\partial\epsilon}\frac{\partial}{\partial\epsilon}\left(\frac{\partial n}{\partial\epsilon} - \frac{n}{2\epsilon}\right) + \epsilon^{-1/2}\psi\left(\frac{\partial n}{\partial\epsilon} - \frac{n}{2\epsilon}\right)\right], \tag{B1}$$

where

$$\psi(\epsilon, t) = 3\int_0^\epsilon n\, dx - (1/\epsilon)\int_0^\epsilon xn\, dx + 2\epsilon^{1/2}\int_\epsilon^\infty x^{-1/2} n\, dx,$$

$$\alpha = \tfrac{2}{3}\pi e^4 (2/m)^{1/2} \ln\Lambda,$$

$$\Lambda = \frac{(kT/4\pi n_0 e^2)^{1/2}}{2e^2/mv^2}$$

and other quantities are the same as defined previously. Defining a new function

$$f(\epsilon) = \epsilon^{-1/2} n/n_0, \quad n_0 = \int_0^\infty n(\epsilon)\, d\epsilon \tag{B2}$$

and substituting into Eq. (B1) yields

$$\frac{\partial n}{\partial t} = \alpha n_0^2 F(\epsilon, t), \tag{B3}$$

where

$$F(\epsilon, t) = 2\epsilon^2 \frac{\partial^2 f}{\partial\epsilon^2}\frac{\partial\varphi}{\partial\epsilon} + \frac{\partial f}{\partial\epsilon}\left(\epsilon\frac{\partial\phi}{\partial\epsilon} + \phi\right) + 3\epsilon^{1/2} f^2$$

and

$$\phi = \psi/n_0.$$

Equation (B1) is equivalent to the formulation of electron-electron interactions presented by Dreicer as Eq. (43) of Ref. 25. It has been shown in

Ref. 26 that this formulation is equivalent to expressing the Coulomb collision integral as the momentum-space divergence of a current density as suggested by Landau.[27] In the present application, where asymmetries in the velocity distribution have been assumed to be negligible, this may be reduced to a divergence in energy space where the appropriate current density is readily obtained by formally writing Eq. (B3) in a flux divergent form

$$\frac{\partial n}{\partial t} = -\frac{\partial J_{ee}}{\partial \epsilon} . \tag{B4}$$

The energy flux due to e-e interactions is $J_{ee} = -\alpha n_0^2 G(\epsilon, T)$ and

$$G(\epsilon, t) = \int_0^{\epsilon} F(x, t)\, dx.$$

Performing the indicated integration of $F(x, t)$ by parts clearing $\partial f/\partial x$ terms, evaluating the resulting partial derivatives of ϕ, and converting from $f(\epsilon, t)$ back to $n(\epsilon, t)$ using Eq. (B2), one obtains the desired results:

$$\frac{\partial n}{\partial t}(\epsilon, t) = -\frac{\partial J_{ee}}{\partial \epsilon} ,$$

$$J_{ee} = \alpha\left[P\left(\frac{n}{2\epsilon} - \frac{\partial n}{\partial \epsilon}\right) - Qn\right] \tag{B5}$$

where

$$P(\epsilon, t) \equiv 2\epsilon^{-1/2} \int_0^{\epsilon} x n(x, t)\, dx + 2\epsilon \int_{\epsilon}^{\infty} x^{-1/2} n(x, t)\, dx,$$

$$Q(\epsilon, t) \equiv 3\epsilon^{-1/2} \int_0^{\epsilon} n(x, t)\, dx.$$

As before, Eq. (B5) is rendered discrete by projecting it onto a finite-differenced energy axis resulting in

$$\frac{\partial n_k}{\partial t} = -\frac{J_{ee}^{+} - J_{ee}^{-}}{\Delta \epsilon} \tag{B6}$$

where

$$J_{ee}^{+}(k) = \alpha\left[\frac{P_{k+1} + P_k}{2}\left(\frac{n_{k+1} + n_k}{4\epsilon_{k+1/2}} - \frac{n_{k+1} - n_k}{\Delta \epsilon}\right) - \frac{Q_{k+1} + Q_k}{2}\,\frac{n_{k+1} + n_k}{2}\right]$$

and

$$J_{ee}^{-}(k) = J_{ee}^{+}(k-1).$$

When the finite-difference Eqs. (B6) are subjected to the boundary condition $J_{ee}^{-}(1) = J_{ee}^{+}(K) = 0$, the desired property of conservation of particles in an isolated system is retained. However the stationality of a Maxwellian distribution and conservation of energy are not automatically preserved to all orders by the finite-difference equations. The remainder of this section will describe how Eq. (B6) is modified to incorporate these properties.

Substitute the expressions for J_{ee}^{+} and J_{ee}^{-} into Eq. (B6) and group terms to find coefficients of n_{k+1}, n_k and n_{k-1}, thus deriving the difference equation

$$\dot{n}_k = a'_{k-1} n_{k-1} + b'_{k+1} n_{k+1} - (a'_k + b'_k) n_k ,$$

where

$$a'_k = \sum_l A_{kl} n_l , \quad b'_k = \sum_l B_{kl} n_l \tag{B7}$$

and

$$A_{kl} = \alpha\{(\epsilon_{k+1}^{-1/2} H_{k+1,l} + \epsilon_k^{-1/2} H_{k,l})(\epsilon_l u_k^{+} - 0.75) + [(1 - H_{k,l})\epsilon_{k+1} + (1 - H_{k-1,l})\epsilon_k](\epsilon_l^{-1/2} u_k^{+})\},$$

$$B_{k+1,l} = \alpha\{(\epsilon_{k+1}^{-1/2} H_{k+1,l} + \epsilon_k^{-1/2} H_{k,l})(\epsilon_l u_k^{-} + 0.75) + [(1 - H_{kl})\epsilon_{k+1} + (1 - H_{k-1,l})\epsilon_k](\epsilon_l^{-1/2} u_k^{-})\}.$$

In the expressions for A_{kl} and $B_{k+1,l}$,

$$u_k^{\pm} = \left(\frac{1}{\Delta \epsilon} \pm \frac{0.25}{\epsilon_{k+1/2}}\right), \quad H_{kl} = \begin{cases} 0, & k < l \\ 1, & k \geq l \end{cases} .$$

The matrix element A_{kl} may be interpreted as the rate (cm^3/sec) for excitation of electrons from ϵ_k to ϵ_{k+1} while electrons at ϵ_l go to ϵ_{l-1}. Similarly B_{kl} is the rate for deexcitation from ϵ_k to ϵ_{k-1} by electrons ϵ_l going to ϵ_{l+1}. The time rate of change of electron energy density is

$$\dot{E} = \sum_{k=1}^{K} \epsilon_k \dot{n}_k \Delta \epsilon,$$

which from Eq. (B7) is

$$\dot{E} = \sum_{kl} (A_{kl} - B_{kl}) n_k n_l (\Delta \epsilon)^2. \tag{B8}$$

Thus from Eq. (B8), $\dot{E}$ is identically zero in an isolated system if

$$\sum_{kl} (A_{kl} - B_{kl}) = 0,$$

which implies that $(A_{kl} - B_{kl})$ is an antisymmetric matrix. Therefore for energy conservation it is sufficient to require that the differenced expressions for A_{kl} and B_{kl} be altered so that

$$A_{kl} = B_{lk} , \tag{B9}$$

and from the physical interpretation of these matrix elements one must also impose the boundary

condition

$$0 = A_{j1} = B_{jK} = A_{Kj} = B_{1j} \quad (j = 1, k). \tag{B10}$$

Finally it remains to be assured that $\dot{\bar{n}}_k = 0$ when $\bar{n}_k$ is a Maxwellian distribution. From the reaction-rate interpretation of A_{jk} and B_{jk} one is led by detail balance to assume at equilibrium

$$\begin{aligned} A_{jk}\bar{n}_j\bar{n}_k &= A_{k-1,j+1}\bar{n}_{k-1}\bar{n}_{j+1} \\ &= B_{j+1,k-1}\bar{n}_{k-1}\bar{n}_{j+1} \end{aligned} \tag{B11}$$

by Eq. (B9). Now substitute Eq. (B9) into Eq. (B7) to obtain

$$\begin{aligned} \dot{\bar{n}}_k = &\sum_{j=1}^{K} (A_{k-1,j}\bar{n}_{k-1}\bar{n}_j - A_{jk}\bar{n}_k\bar{n}_j) \\ &+ \sum_{j=1}^{K} (A_{j,k+1}\bar{n}_{k+1}\bar{n}_j - A_{kj}\bar{n}_k n_j) \end{aligned} \tag{B12}$$

for $2 \leq k \leq K-1$. Consider the first sum in Eq. (B12) using Eq. (B11)

$$\sum_{j=1}^{K} A_{k-1,j}\bar{n}_{k-1}\bar{n}_j = \sum_{j=1}^{K} A_{j-1,k}\bar{n}_{j-1}\bar{n}_k ,$$

which with Eq. (B10) equals

$$\sum_{j=2}^{K} A_{j-1,k}\bar{n}_{j-1}\bar{n}_k = \sum_{j=1}^{K-1} A_{j,k}\bar{n}_j\bar{n}_k ;$$

Using Eq. (B10) and (B11) again, this gives

$$\sum_{j=1}^{K} A_{k-1,j}\bar{n}_{k-1}\bar{n}_j = \sum_{j=1}^{K} A_{j,k}\bar{n}_j\bar{n}_k ,$$

and hence the first sum on the right-hand side of Eq. (B12) vanishes identically. Similarly the second sum is reduced

$$\begin{aligned} \sum_{j=1}^{K} A_{j,k+1}\bar{n}_{k+1}\bar{n}_j &= \sum_{j=1}^{K-1} A_{k,j+1}\bar{n}_k n_{j+1} = \sum_{j=2}^{K} A_{k,j}\bar{n}_k\bar{n}_j \\ &= \sum_{j=1}^{K} A_{k,j}\bar{n}_k\bar{n}_j \end{aligned}$$

so that $\dot{\bar{n}}_k = 0$ for $2 \leq k \leq K-1$. In a like manner it can be shown to be true for $k=1$ and $k=K$, thus the relationship

$$A_{j,k} = A_{k-1,j+1}(\epsilon_{k-1}/\epsilon_k)^{1/2}(\epsilon_{j+1}/\epsilon_j)^{1/2} \tag{B13}$$

set by Eq. (B11) when $\bar{n}_k$ is a Maxwellian quarantees that a Maxwellian distribution is a steady-state solution of Eq. (B6). This concludes the formal development of e-e interactions into a flux divergent difference equation.

---

*Work performed under the auspices of the United States Atomic Energy Commission.

[1]N. G. Basov, V. A. Danilychev, and Yu. M. Popov, Sov. J. Quantum Electron 1, 181 (1971).
[2]See, for example, (a) A. G. Engelhardt and A. V. Phelps, Phys. Rev. 131, 2115 (1963); (b) A. G. Englehardt, A. V. Phelps, and C. G. Risk, Phys. Rev. 135, A1566 (1964) and work cited therein.
[3]W. L. Nighan, Phys. Rev. A 2, 1989 (1970).
[4]S. D. Rockwood, J. E. Brau, G. H. Canavan, and W. A. Proctor, IEEE J. Quantum Electron 9, 120 (1973).
[5]J. H. Wilkinson, *The Algebraic Eigenvalue Problem* (Clarendon, Oxford, 1965).
[6]W. A. Proctor and G. H. Canavan, Bull. Am. Phys. Soc. 17, 979 (1972).
[7]See, for example, W. E. Milne, *Numerical Solution of Differential Equations* (Wiley, New York, 1953).
[8]C. W. McCutchen, Phys. Rev. 112, 1848 (1958).
[9]W. L. Borst, Phys. Rev. 181, 257 (1969).
[10]H. Harrison, thesis (unpublished), data quoted by L. J. Kieffer and G. H. Dunn, Rev. Mod. Phys. 38, 1 (1966).
[11]T. W. Ottley, D. R. Denne, and H. Kleinpoppen, Phys. Rev. Lett. 29, 1646 (1972).
[12]A. von Engel, *Ionized Gases*, 2nd ed. (Oxford U. P., Oxford, 1965).
[13]V. A. Ovcharenko and S. M. Chernyshev, Teplofiz. Vys. Temp. 8, 716 (1970) [High Temp. 8, 679 (1970)].
[14]E. Hayes and K. Wojacyek, Beitr. Plasma Phys. 3, 74 (1963).
[15]B. Klarfeld, Tech. Phys. (USSR) 5, 913 (1938).
[16]D. E. Davies and D. Smith, Brit. J. Appl. Phys. 16, 697 (1965).
[17]G. D. N. Overton and D. E. Davies, J. Phys. D 1, 881 (1968).
[18]P. C. Johnson and A. B. Parker, Proc. Roy. Soc. A 325, 529 (1971).
[19]C. Kenty, J. Appl. Phys. 21, 1309 (1950).
[20]R. B. Brode, Proc. Roy. Soc. A 125, 134 (1929).
[21]J. H. Simons and R. P. Seward, J. Chem. Phys. 6, 790 (1938).
[22]A. Atajew, A. Rutscher, and R. Winkler, Beitr. Plasma Phys. 12, 239 (1972).
[23]W. P. Allis, *Handbuch der Physik*, (Springer-Verlag, Berlin, 1956), Vol. XXI.
[24]M. N. Rosenbluth, W. M. MacDonald, and D. L. Judd, Phys. Rev. 107, 1 (1957).
[25]H. Dreicer, Phys. Rev. 117, 343 (1960).
[26]L. R. Megill and J. H. Cahn, J. Geophys. Res. 69, 5041 (1964).
[27]L. Landau, Phys. Z. Soviet Union 10, 154 (1936).